Localization of MMR proteins on meiotic chromosomes in mice indicates distinct functions during prophase I

Nadine K. Kolas,[1] Anton Svetlanov,[1] Michelle L. Lenzi,[1] Frank P. Macaluso,[2] Steven M. Lipkin,[5] R. Michael Liskay,[6] John Greally,[1,3] Winfried Edelmann,[4] and Paula E. Cohen[1]

[1]Department of Molecular Genetics, [2]Department of Anatomy and Structural Biology, [3]Department of Medicine, and [4]Department of Cell Biology, Albert Einstein College of Medicine, Bronx, NY 10461
[5]Department of Hematology, University of California, Irvine, Irvine, CA 92697
[6]Molecular and Medical Genetics, Oregon Health Sciences University, Portland, OR 97239

Mammalian MutL homologues function in DNA mismatch repair (MMR) after replication errors and in meiotic recombination. Both functions are initiated by a heterodimer of MutS homologues specific to either MMR (MSH2–MSH3 or MSH2–MSH6) or crossing over (MSH4–MSH5). Mutations of three of the four MutL homologues (*Mlh1*, *Mlh3*, and *Pms2*) result in meiotic defects. We show herein that two distinct complexes involving MLH3 are formed during murine meiosis. The first is a stable association between MLH3 and MLH1 and is involved in promoting crossing over in conjunction with MSH4–MSH5. The second complex involves MLH3 together with MSH2–MSH3 and localizes to repetitive sequences at centromeres and the Y chromosome. This complex is up-regulated in $Pms2^{-/-}$ males, but not females, providing an explanation for the sexual dimorphism seen in $Pms2^{-/-}$ mice. The association of MLH3 with repetitive DNA sequences is coincident with MSH2–MSH3 and is decreased in $Msh2^{-/-}$ and $Msh3^{-/-}$ mice, suggesting a novel role for the MMR family in the maintenance of repeat unit integrity during mammalian meiosis.

Introduction

The eukaryotic DNA mismatch repair (MMR) family repairs a variety of mismatches and also participates in reciprocal recombination events during meiosis (Kolodner, 1996; Modrich, 1997; Kirkpatrick, 1999). MMR activity is initiated by the detection of a substrate by a heterodimer of MutS homologues (MSHs), of which there are five in mammals, MSH2 through MSH6. They form three heterodimeric complexes: MSH2–MSH6 (MutSα), MSH2–MSH3 (MutSβ), and MSH4–MSH5 (MutSγ). Of these, MutSα initiates the repair of base–base and insertion–deletion mispairs, whereas MutSβ participates in the repair of only the latter (Nakagawa et al., 1999). The meiosis-specific MutSγ complex is crucial for reciprocal recombination in yeast (Ross-Macdonald and Roeder, 1994; Hollingsworth et al., 1995; Winand et al., 1998), nematodes (Zalevsky et al., 1999), and mice (de Vries et al., 1999; Edelmann et al., 1999; Kneitz et al., 2000), but has no MMR activity per se.

After MutS association with the DNA, a heterodimeric complex of MutL homologues is recruited. Four mammalian MutL homologues exist, but the principal heterodimers that function in mitotic repair and meiotic reciprocal recombination are MLH1–PMS2 (postmeiotic segregation 2) and MLH1–MLH3, respectively (Kolodner and Marsischky, 1999; Flores-Rozas and Kolodner, 2000), whereas in yeast these heterodimers are represented by Mlh1–Pms1 and Mlh1–Mlh3 (Nakagawa et al., 1999; Wang et al., 1999; Hoffmann and Borts, 2004).

The mammalian meiotic MMR complex, consisting of MSH4, MSH5, MLH1, and MLH3, has been implicated in the processing of DNA double strand breaks (DSB) through the double Holliday junction (dHJ) recombination intermediate repair pathway that results in reciprocal crossover events between parental homologous chromosomes (Ross-Macdonald and Roeder, 1994; Hollingsworth et al., 1995; Novak et al., 2001; Borner et al., 2004; Hoffmann and Borts, 2004; Surtees et al.,

Nadine K. Kolas and Anton Svetlanov contributed equally to this work.
Correspondence to P.E. Cohen: pc242@cornell.edu
P.E. Cohen's present address is Dept. of Biomedical Sciences, Cornell University, Ithaca, NY 14853.

Abbreviations used in this paper: DDB, double dense body; dHJ, double Holliday junction; DSB, DNA double strand break; MLH1 and 3, MutL homologue 1 and 3; MMR, mismatch repair; MN, meiotic nodule; MSH2–6, MutS homologue; PAR, pseudoautosomal region; PMS2, postmeiotic segregation 2; TNR, trinucleotide repeat.

The online version of this article includes supplemental material.

The Journal of Cell Biology, Vol. 171, No. 3, November 7, 2005 447–458
http://www.jcb.org/cgi/doi/10.1083/jcb.200506170

2004). Studies in mouse (Kneitz et al., 2000; Santucci-Darmanin et al., 2000; Moens et al., 2002) and human germ cells (Lenzi et al., 2005) show that MSH4–MSH5 appear at recombination intermediates, as part of the multiprotein meiotic nodule (MN), early in prophase I and accumulate at frequencies that far exceed the eventual number of crossover sites (Kneitz et al., 2000). In vitro biochemical studies suggest that this heterodimer forms a sliding clamp that associates with dHJ structures at zygonema (Snowden et al., 2004) a subset of which may be stabilized by interactions with MLH1–MLH3 heterodimers at pachynema. It is these sites that will eventually become the crossovers that ensure accurate chromosomal segregation at the first meiotic division. The additional MSH4–MSH5 sites that are not stabilized by MLH1–MLH3 are then repaired through noncrossover mechanisms.

The temporal dynamics of MMR protein association with MNs raises the question of how MLH1 and MLH3 selects only a subset of MSH4–MSH5 sites to become crossover events. Previous studies have demonstrated that MLH3-only foci are apparent during pachynema of prophase I, whereas MLH1 appearance at crossovers is dependent on MLH3 (Lipkin et al., 2002). This suggests an MLH3-driven mechanism for dHJ selection. Alternatively, the involvement of a third MutL homologue, PMS2, has been suggested, at least in males, by the observation that *Pms2*$^{-/-}$ males are sterile, whereas females remain fertile (Baker et al., 1995). By contrast, mutation of *Mlh1* or *Mlh3* results in sterility of both males and females (Baker et al., 1996; Edelmann et al., 1996; Woods et al., 1999; Lipkin et al., 2002). Interestingly, however, although germline crossover rates are decreased to ~10% in male and female mice lacking *Mlh1* (Baker et al., 1996; Woods et al., 1999), they appear to be unaffected in male mice lacking *Pms2* (Qin et al., 2002). Because MLH1 is capable of heterodimerizing with both MLH3 and PMS2, this prompted us to explore the interactions between these MutL homologues at the chromosomal level in spermatocytes from wild-type mice, and from *Mlh1*-, *Mlh3*-, and *Pms2*-null animals.

Using a variety of cytological and molecular techniques, we present genetic evidence that MLH3 associates with complexes involving both MSH2–MSH3 and MSH4–MSH5 in mammalian meiocytes, and that only the latter is necessary for reciprocal recombination. A second complex, consisting of MutSβ (MSH2–MSH3) together with MLH3, associates with regions of the genome that are rich in repetitive sequences, such as the major and minor satellites of the centromere region and the Y chromosome, suggesting a new role for MMR complexes in the mammalian germline.

Results

Temporal dynamics of MutL association with MN during recombination

The synaptonemal complex (SC) is the tripartite protein structure that forms a continuous filament structure along homologous chromosomes and tethers them together during prophase I (Page and Hawley, 2004). The SC also serves as the docking site for key recombinational proteins of the MN. To assess the dynamics of MutL homologue accumulation through prophase I, MLH1 and MLH3 were localized to SCs of mouse spermatocytes. MLH3 foci are found on the SC of wild-type spermatocytes from early pachynema (Fig. 1, A and B), but MLH1 does not associate with MLH3 until mid-pachynema (Fig. 1, A and B). The early MLH3 foci probably account for the few instances of MLH3-positive, MLH1-negative foci reported in our previous studies (Lipkin et al., 2002), that we suggest then recruit MLH1 in mid-pachynema. MLH1 and MLH3 persist through to late pachynema and are rarely seen at diplonema. The number of MLH1–MLH3 foci correlates well with the predicted number of crossovers in mouse spermatocytes (Anderson et al., 1999), suggesting that MLH1–MLH3 marks most, if not all, of the reciprocal recombination sites during mouse meiosis, and making it less likely that MLH1–PMS2 heterodimers are marking another subset of such sites.

The MLH1–MLH3 localization pattern does not exclude the possibility of other PMS2 effects on meiotic progression. However, despite trying at least eight different anti-PMS2 antibodies, generated by our laboratory and others, it has not been possible to localize PMS2 in meiotic chromosome preparations. Instead, we examined the distribution of MLH1 and MLH3 on SCs from *Pms2*$^{-/-}$ spermatocytes and found that both localize to the SCs at EM-defined MNs, with near normal temporal (Fig. 1, C and D) and spatial frequency. MLH1 accumulates slightly earlier in the absence of PMS2 than in spermatocytes from wild-type males (Fig. 1 D) but is still always found in combination with MLH3. The eventual number of MLH1 and MLH3 observed at late pachynema in *Pms2*$^{-/-}$ spermatocytes is slightly (and, in the case of MLH1, significantly) higher than that seen in wild-type spermatocytes (Fig. 1, D and E; $P = 0.033$ and 0.077 by Mann-Whitney U test, for MLH1 and MLH3, respectively). The normal accumulation of MLH1 and MLH3 on SCs of *Pms2*$^{-/-}$ males is associated with the persistence of MN structures, as observed at the EM level (Fig. 1 C), and with normal chiasma counts at metaphase I in these mice (unpublished data).

Our previous studies demonstrated that MLH1 fails to localize to SCs in spermatocytes from *Mlh3*$^{-/-}$ males and that this was associated with loss of MNs at pachynema and absence of crossovers at metaphase (Lipkin et al., 2002). In view of the temporal dissociation of MLH1 and MLH3 accumulation observed in the current study, we hypothesized that MLH3 foci might localize independently of MLH1 on SCs from *Mlh1*$^{-/-}$ spermatocytes. Indeed, immunogold-labeled SCs from *Mlh1*$^{-/-}$ spermatocytes revealed large residual MNs that were loaded with MLH3 (Fig. 1 F). Quantitation of MLH3- and MLH1-containing foci (by immunofluorescence microscopy) on SCs from spermatocytes of all MMR genotypes confirmed this observation, demonstrating that accumulation of MLH3 in *Mlh1*$^{-/-}$ spermatocytes occurs at a significantly lower frequency than that in wild-type spermatocytes (Fig. 1 E; $P < 0.0001$ by Mann-Whitney U test), whereas MLH1 fails to localize at all on SCs of *Mlh3*$^{-/-}$ spermatocytes, as described previously (Fig. 1 E; Lipkin et al., 2002).

Localization of MLH3, and occasionally MLH1, with CREST-positive regions of wild-type and Pms2$^{-/-}$ male chromosomes reveals an unexpected centromere-associated MMR complex

In view of the apparently normal recombination frequency in spermatocytes of *Pms2*$^{-/-}$ males (Fig. 1; Qin et al., 2002), we investigated whether other MMR-related functions might be disrupted in these animals. Examination of the SCs from *Pms2*$^{-/-}$ males by EM revealed an accumulation of both MLH1 and MLH3 close to the centromere (Fig. 2 A), a region that is usually not subject to crossing over (Broman et al., 1998; Froenicke et al., 2002) and is therefore not expected to be positive for this MutL complex. Examination of the centromere regions from other MMR-deficient mouse strains revealed similar, but reduced frequency of, localization of MLH3 in spermatocytes from wild-type (Fig. 2 B) and *Mlh1*$^{-/-}$ males (Fig. 2 C), but not from *Mlh3*$^{-/-}$ males (Fig. 2 D). In wild-type and *Mlh1*$^{-/-}$ males, MLH3 associated with ~15–25% of all spermatocyte autosomal centromeres. Little if any MLH1 was associated with centromere regions in wild-type, *Mlh1*$^{-/-}$, or *Mlh3*$^{-/-}$ mice (Fig. 2, B–E). The localization of MLH3 at centromeres increased to include >85% of centromere regions in spermatocytes from *Pms2*$^{-/-}$ males, and colocalized at most of these sites (>65% of total centromeres) with MLH1 (Fig. 2 E). The EM images of immunogold-labeled spermatocyte spread preparations were supported by similar localization at the immunofluorescence level (Fig. S1 available at http://www.jcb.org/cgi/content/full/jcb.200506170/DC1), but was much weaker using fluorescently-labeled secondary antibodies (which are monoclonal antibodies) than using gold-labeled secondaries (polyclonal antibodies). The EM analysis involves a higher

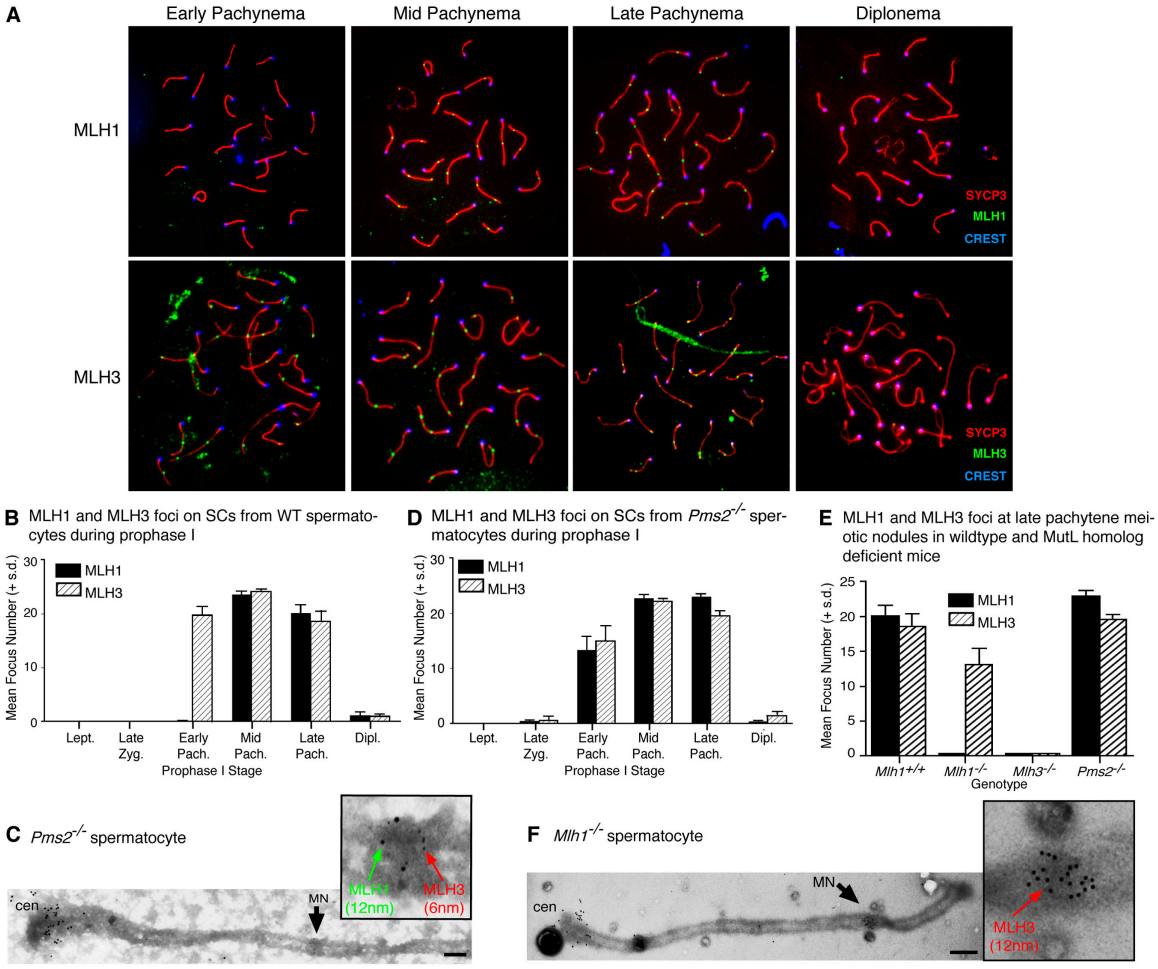

Figure 1. **Expression pattern of MLH3 and MLH1 in spermatocytes from wild-type mice and those with targeted mutations of the MutL homologues.** (A) MLH1 (top; green, FITC) localizes to spermatocyte SCs (SYCP3: red, TRITC) from mid to late pachynema but is not present in early diplonema. MLH3 localizes to SCs earlier than MLH1, during early pachynema, and persists until late pachynema. Centromeres are labeled with CREST (blue, CY5). (B) Quantitation of MLH1 (black bars) and MLH3 (striped bars) on wild-type spermatocyte SCs confirms the earlier localization of MLH3. (C) Immunogold-EM localization of MLH3 (6 nm gold grains) and MLH1 (12 nm gold grains) on *Pms2*$^{-/-}$ spermatocytes demonstrates colocalization to electron-dense MNs (inset) during mid-pachynema. Centromeres (cen) are labeled with CREST (18 nm gold grains). Bar, 200 nm. (D) Quantitation of MLH1 (black bars) and MLH3 (striped bars) localization indicates that MN frequency, as measured by MLH1/3 labeling, is unaffected, or slightly elevated, in *Pms2*$^{-/-}$ spermatocytes. (E) Quantitation of MLH1 and MLH3 foci in spermatocytes from mice with targeted deletions of *Mlh1, Mlh3,* and *Pms2* indicates that even though MLH3 can bind to SCs in the absence of MLH1, MLH1 is incapable of localizing in the absence of MLH3. Neither MLH1 nor MLH3 localization is reduced in the absence of PMS2. (F) Immunogold-EM showing MLH3 (12 nm gold grains) localization to MNs (inset) in the absence of MLH1. Centromeres (cen) are localized with CREST (18 nm gold grains). Bar, 500 nm. Error bars indicate SD.

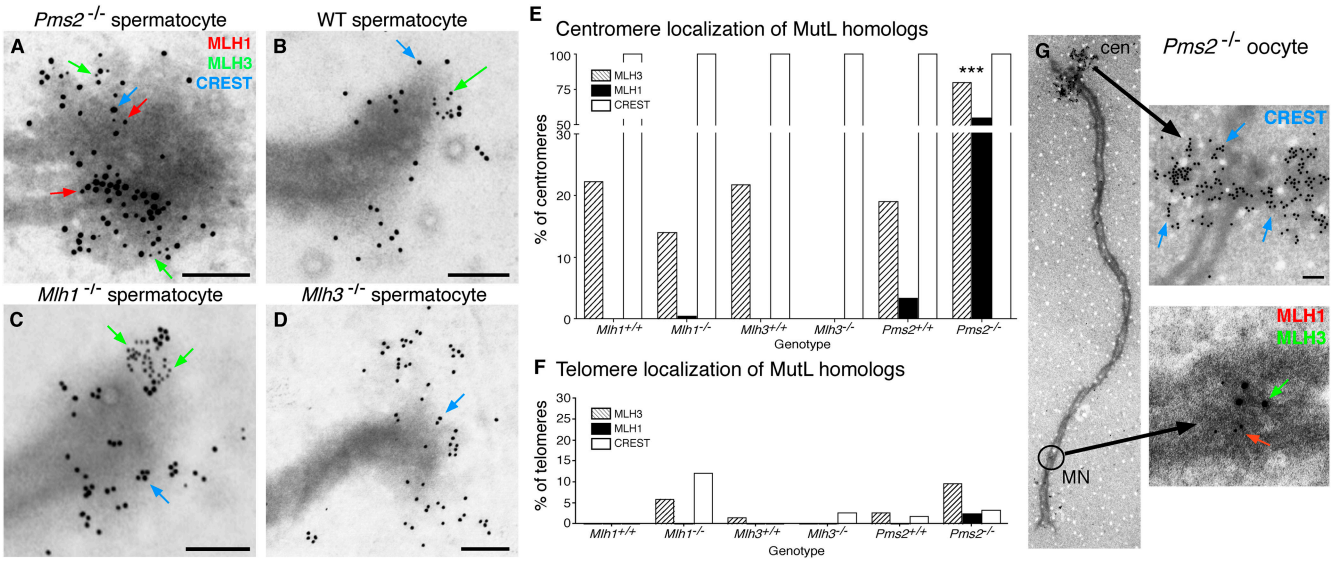

Figure 2. **MLH3 immunolocalizes to a proportion of wild-type and *Mlh1*$^{-/-}$ spermatocyte centromeres, and both MLH3 and MLH1 localize to the centromeres of *Pms2*$^{-/-}$ spermatocytes but not *Pms2*$^{-/-}$ oocytes.** (A–D) Immunogold-EM localization of MLH1 (12 nm gold grains, red arrows), MLH3 (6 nm gold grains, green arrows), and CREST (18 nm gold grains, blue arrows) on meiotic chromosomes of *Pms2*$^{-/-}$ (A), wild-type (B), *Mlh1*$^{-/-}$ (C), and *Mlh3*$^{-/-}$ (D) spermatocytes. Bars: (A, B, and D) 250 nm; (C) C 500 nm. All SCs are counterstained with phosphotungstic acid. (E) Quantitation of MMR protein localization to centromeres from *Mlh1*$^{+/+}$, *Mlh1*$^{-/-}$, *Mlh3*$^{+/+}$, *Mlh3*$^{-/-}$, *Pms2*$^{+/+}$, and *Pms2*$^{-/-}$ spermatocytes. Counts were obtained from immunogold-EM micrographs exemplified in A–D and represent those centromeres showing more than four gold grains for each antibody staining. At least 100 centromeres were counted for each genotype from three mice. Percentages represent pooled counts from all these mice. MLH3 (striped bars) immunolocalizes to 15–25% of wild-type and *Mlh1*$^{-/-}$, but not *Mlh3*$^{-/-}$, spermatocyte centromeres. MLH1 (black bars) does not localize in any appreciable amount to centromeres in wild-type, *Mlh1*$^{-/-}$ or *Mlh3*$^{-/-}$ spermatocytes. CREST (white bars) localizes to 100% of the centromeres. *Pms2*$^{-/-}$ spermatocyte centromeres show a statistically significant increase in localization of both MLH1 and MLH3 in comparison with the *Pms2*$^{+/+}$ and all other mouse strains observed. (F) Quantitation of distal (noncentromeric) telomere localization (more than four gold grains) indicates that the localization of MutL homologues is specific to the centromere. (G) EM micrograph of MLH1 (6 nm gold grains) and MLH3 (12 nm gold grains) on SCs from *Pms2*$^{-/-}$ oocytes indicates that, whereas MLH3 and MLH1 localize normally to MNs (bottom inset), these MutL homologues fail to localize to the centromere (cen), labeled with CREST (18 nm gold grains; top inset). Bar, 200 nm.

concentration of primary antibody, coupled with DNaseI digestion of heterochromatin to improve accessibility of the antibodies to the centromere sites, perhaps explaining the difference in staining intensity.

Considering mouse centromeres are telocentric, we examined whether the accumulation of MLH1–MLH3 at the centromere region in *Pms2*$^{-/-}$ spermatocytes was due to the centromere per se or the closely-adjacent telomere. We did not observe elevated MLH1–MLH3 accumulation at the distal telomere of *Pms2*$^{-/-}$ males (Fig. 2 F). Moreover, the Y chromosome, which has a larger expanse between the proximal telomere and the centromere, showed specific accumulation to the centromeric region (Fig. 3), leading us to conclude that the accumulation of MLH3 at these regions was associated specifically with centromere-associated sequences. The presence of MLH3 at centromere regions in wild-type and *Mlh1*$^{-/-}$ spermatocytes indicates that MLH3 is able to localize to the chromosome independently of MLH1, as it does at early MNs (Fig. 1, B and C).

Localization of MLH3 and MLH1 at centromeric regions is associated with major and minor satellite repeat sequences

The mammalian centromere is a highly specialized structure consisting of protein-associated centromeric sequences and adjacent minor satellite DNA flanked by pericentric major satellite DNA (Guenatri et al., 2004). Major/minor satellites are regions of highly repetitive heterochromatin-forming sequences that are important for centromere function associated with spindle attachment and sister chromatid cohesion. In mice, the major satellite consists of tandem repeats of 234-bp units, of which there are ~700,000 copies per cell, reflecting an average of 35,000 copies per chromosome (totaling 8 MB in length; Horz and Altenburger, 1981). The minor satellite binds histone H3 and CENPA/B, is present in 50–100,000 copies, and appears to share common ancestry with the major satellite (Silver, 1995). In humans, similar repeats of ~171 bp are present but are termed α satellites (Muro et al., 1992).

The localization of MLH3 (and in some cases, MLH1) at the centromere prompted us to investigate the specificity of this association with centromere-associated repeats. We performed chromatin immunoprecipitation (ChIP) experiments using either crude germ cell extracts (consisting of mixed populations of germ cells) or isolated pachytene spermatocytes (estimated to be >95% pure). MLH3-containing complexes were immunoprecipitated using an anti-MLH3 antibody, followed by amplification using degenerate oligonucleotide PCR (Telenius et al., 1992) and subsequent slot-blot analysis using PCR-generated probes specific to mouse major and/or minor satellite sequences (Garagna et al., 2002). A B2 SINE element probe was used as a loading control (Serdobova and Kramerov,

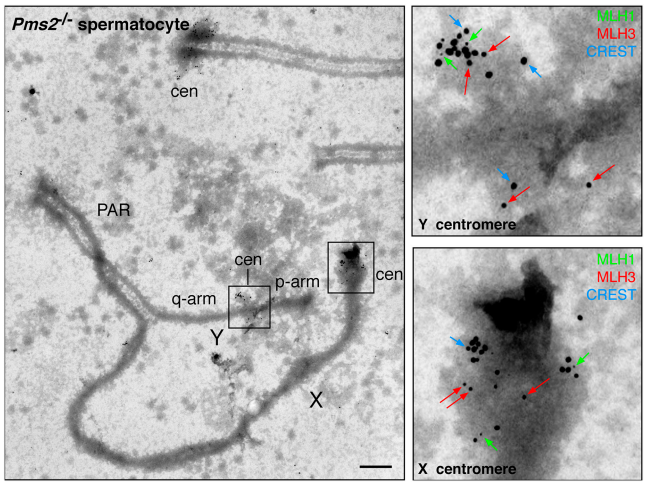

Figure 3. **Localization of MLH1 and MLH3 to Y chromosome centromere region.** Immunogold-EM localization of MLH1 (6 nm gold grains, green arrows), MLH3 (12 nm gold grains, red arrows), and CREST (18 nm gold grains, blue arrows) on meiotic chromosome cores of *Pms2*$^{-/-}$ sex chromosomes. The p-arm of the Y chromosome is cytologically distinct from the q-arm, which contains the PAR that synapses with the PAR of the X chromosome. Due to the length of the p-arm, the Y chromosome centromere (top inset) can be differentiated from the terminally located telomere and both MLH1 and MLH3 localize to both the X (bottom inset) and the Y chromosome centromere. SCs are counterstained with phosphotungstic acid. Bar, 500 nm.

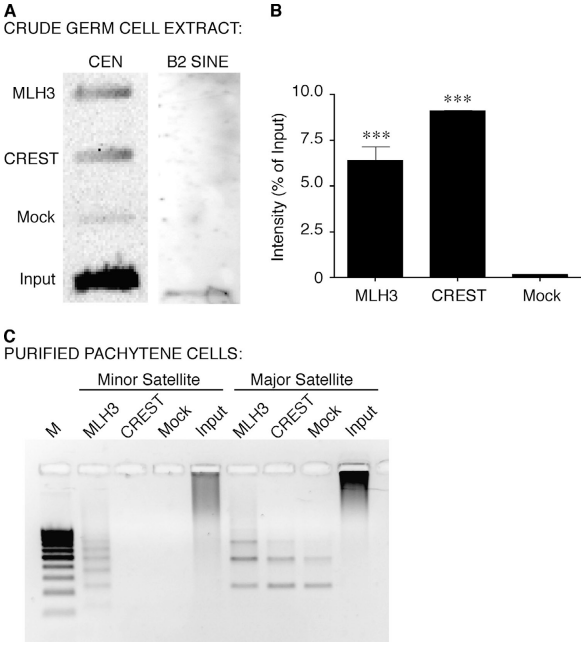

Figure 4. **Chromatin immunoprecipitation of centromere-associated repeat sequences by antibodies against MMR proteins.** (A) Representative slot blot analysis of major and minor satellite repeat sequences (CEN) performed on crude germ cell lysates immunoprecipitated with antibodies MLH3, CREST, or rabbit IgG (Mock control), compared with input DNA. The same slot blot membrane was stripped and reprobed with a B2 SINE probe as a loading control. (B) Quantitation of three centromere ChIP experiments, expressed as a percentage of input DNA + SD. Statistical analysis was performed using unpaired *t*-tests (***$P < 0.0001$). (C) ChIP assay followed by PCR using primers against minor and major satellite sequences performed on purified pachytene cells from *Pms2*$^{-/-}$ testes. Lanes (from left to right): lane 1, molecular weight marker; lanes 2–5, minor satellite PCR; lanes 6–9, major satellite PCR. M, 100 bp marker; Input, input DNA. 10-fold dilutions of ChIP pull-down substrate DNA was used for minor satellite PCR, DNA for major satellite PCR was undiluted.

1998), representing a ubiquitous genome-wide repeat element, and showing that MLH3 does not bind to all repeat sequences throughout the genome.

ChIP of mixed germ cell extracts from *Pms2*$^{-/-}$ males with the anti-MLH3 antibody enriched centromeric major/minor satellite sequences above control levels at comparable rates to that seen for polyclonal CREST serum, which recognizes a variety of CENPs (Fig. 4, A and B). The enrichment of centromere repeats in *Pms2*$^{-/-}$ spermatocytes with anti-MLH3 antibody or with CREST was statistically elevated compared with mock controls (unpaired *t* tests, $P < 0.0001$). No enrichment of similar regions was found in ChIP extracts from *Mlh1*$^{-/-}$ and *Mlh3*$^{-/-}$ males, although specificity of enrichment was confirmed by PCR of random genomic sequences (β-actin) using the same immunoprecipitates (Fig. S2 available at http://www.jcb.org/cgi/content/full/jcb.200506170/DC1).

To examine the specific contribution of major and minor satellite sequences to the observed MLH3 association, purified populations of *Pms2*-null spermatocytes were subjected to ChIP using anti-MLH3 antibody, followed by PCR to amplify banded sequences specific to each satellite. MLH3 associates specifically with both minor and major satellite sequences (Fig. 4 C, lanes 2 and 6), along with CREST immunoserum (Fig. 4 C, lanes 3 and 7). The enrichment of major and minor sequences by MLH3 or CREST immunosera was significantly raised above mock (no antibody) controls, although was greater for the MLH3 enrichment of minor satellites than either the MLH3 or CREST enrichment of major satellite sequences. CREST enrichment of minor sequences was barely visible because of the extent of the dilution required to optimize the MLH3 signal.

Association of MLH3 on the nonpseudoautosomal region of the Y chromosome

To investigate the association of the MMR machinery with other repetitive sequences in the genome, we explored the localization of MLH3 across the Y chromosome, which in humans and mice contains large palindromic repeat sequences (Bishop et al., 1985; Singh et al., 1994; Rozen et al., 2003; Skaletsky et al., 2003) and which, like the centromere, is refractory to reciprocal recombination except at the X-Y pseudoautosomal region (PAR). MLH3 localizes in dense foci along the Y chromosome in some pachytene spermatocytes from wild-type, *Pms2*$^{-/-}$ and *Mlh1*$^{-/-}$ males (Fig. 5 A, *Pms2*$^{-/-}$ example shown), but the localization is not consistent among spermatocyte populations. In total, of the more than 500 nuclei examined from *Pms2*$^{-/-}$ males, ~10% exhibited the Y chromosome accumulation of MLH3. No MLH1 association was found along the Y chromosome in wild-type or in *Pms2*$^{-/-}$ spermatocytes (unpublished data). ChIP analysis confirmed the localization of MLH3 (Fig. 5, B and C), and the absence of MLH1 (unpublished data), on Y chromosome sequences from *Pms2*$^{-/-}$ males.

Association of MutL homologues with repetitive sequences is dependent on MutSβ (MSH2-MSH3) but independent of MutSγ (MSH4-MSH5)

The observations outlined above indicate that MLH3 localizes to centromere repetitive sequences and the Y chromosome in spermatocytes from wild-type mice, and hyperlocalizes to centromeric regions, along with MLH1, when PMS2 is absent. That both of these sites do not usually undergo reciprocal exchange suggests that the DNA-binding MutS partners for MLH3 at these sites are not the MSH4–MSH5 heterodimers that are usually only associated with DSB-induced recombination intermediates in meiotic cells. Therefore, we hypothesized that another MSH2-containing MutS heterodimer could be associated with these sites. In view of yeast genetic data demonstrating that Mlh3 associates with MutSβ (MSH2–MSH3) heterodimers (and not MutSα, MSH2–MSH6) to effect repair (Flores-Rozas and Kolodner, 1998), this complex was the most obvious choice for investigation.

Immunofluorescence analysis of chromosome preparations from wild-type spermatocytes demonstrated that MSH2 and MSH3 localize strongly to the centromere (Fig. 6, A–F) and on the sex chromosomes (Fig. 6, C and F, arrows), and that this localization is as frequent in wild-type spermatocytes as it is in *Pms2*$^{-/-}$ males (Fig. 7, A–C and J). These observations indicate that the association of MSH2–MSH3-containing complexes appear to be a feature of normal prophase I and are not specifically up-regulated in the absence of PMS2. No association of MSH2 with these genomic regions is observed in spermatocytes from *Msh3*$^{-/-}$ males either by immunofluorescence or EM (Fig. 6 G and Fig. 7, D–F), indicating that MSH3 is required for MSH2 localization to these sites. By contrast, immunofluorescence and immunogold localization of MSH2 at the centromere is not affected in spermatocytes from *Msh4*$^{-/-}$, *Msh5*$^{-/-}$, or *Msh6*$^{-/-}$ males (Fig. 6, H and I, and Fig. 7, G–J). MSH2, and to a lesser degree MSH3, localizes along the chromosomes, but at an intensity that is far lower than that seen at the centromere (Fig. 6, A and D, arrowheads; Fig. 7, A and G, arrowheads). This interstitial localization could be the result of canonical MMR activity.

Quantitation of MLH1 and MLH3 association with centromere regions by immunogold-EM in spermatocytes from *Msh2*$^{-/-}$, *Msh3*$^{-/-}$, *Msh5*$^{-/-}$, and *Msh6*$^{-/-}$ males confirmed the requirement for MSH2–MSH3, and not MSH2–MSH6 or MSH4–MSH5, to localize MLH3 to these sites (Fig. 6 J). In *Msh2*$^{-/-}$ males, the localization of MLH3 at sites of reciprocal exchange is normal, but there is a statistically significant decrease in the localization of MLH3 at the centromere, from the usual 15–25% frequency seen in wild-type pachytene spermatocytes to near undetectable levels (Fig. 6 J; chi-square analysis $P < 0.0002$). Similarly, significantly decreased centromere localization of MLH3 is observed in spermatocytes from *Msh3*$^{-/-}$ animals (Fig. 6, G and J; χ^2 analysis $P < 0.0002$), but not in *Msh5*$^{-/-}$ or *Msh6*$^{-/-}$ males (Fig. 6, H–J; χ^2 analysis $P = 0.81$ and $P = 0.04$, respectively). Thus, the association of MLH3 with repeat sequences uses the MSH2–MSH3 complex, whereas MLH1–MLH3 association at MNs uses MSH4–MSH5.

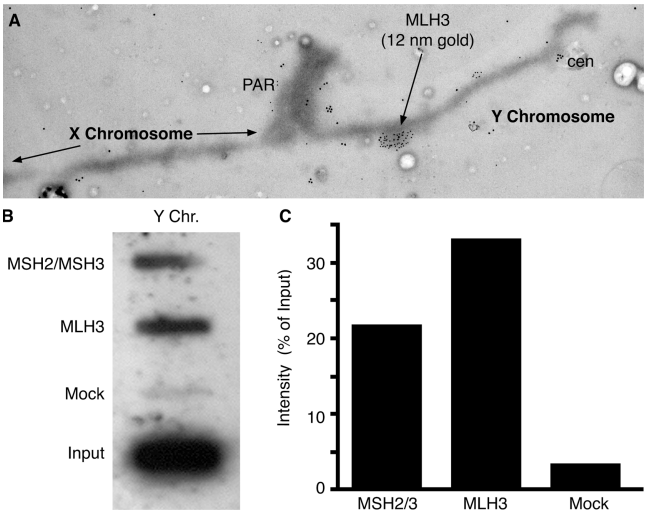

Figure 5. **Localization of MMR complexes on the mouse Y chromosome during prophase I.** (A) Immunogold-EM micrograph of an XY bivalent from a *Pms2*$^{-/-}$ spermatocyte showing the PAR, the entire Y chromosome and part of the X chromosome. MLH3 localization is marked by the presence of 12 nm gold beads, showing a large dense focus on the Y chromosome. The centromere (cen) is marked with CREST labeled with 18 nm gold beads, and the SC is counterstained with phosphotungstic acid. (B) Representative slot blot analysis of Y chromosome repeat sequences immunoprecipitated with antibodies against MutSβ (combined MSH2–MSH3 antibodies; Oncogene Research Products), MLH3, and rabbit IgG (Mock control). (C) Quantitation of ChIP experiment in B, expressed as a percentage of input DNA.

Combined antibodies against MSH2–MSH3 were used in ChIP assays and were shown to enrich sequences within the centromeric (unpublished data) and Y chromosome repeat domains (Fig. 5, B and C). This MSH2–MSH3 enrichment of repetitive sequences is observed in spermatocyte extracts from wild-type males as well as in *Pms2*$^{-/-}$ extracts, whereas MLH3 enrichment is only observed in the absence of PMS2. These data confirm the immunolocalization observations indicating that MSH2–MSH3 is constitutively associated with centromeric repetitive sequences and the Y chromosome. This repeat association appears to be meiosis-specific as no centromeric localization of MSH2–MSH3 or MLH3 was observed in somatic cells in vitro (unpublished data).

Analysis of Msh2$^{-/-}$Pms2$^{-/-}$ double-null males suggests that PMS2 is not acting directly at the centromere region

The meiotic failure observed in *Pms2*$^{-/-}$ males together with the hyperlocalization of MLH1–MLH3 at the spermatocyte centromeres in these mice indicated a role for PMS2 at centromere repeats, possibly dependent on MSH2–MSH3. Confounding this hypothesis, however, is the normal fertility in *Msh2*$^{-/-}$ males. One possible explanation is that MSH2–MSH3 heterodimers act as a repeat tract surveillance mechanism that, under normal circumstances, signals to a PMS2-containing complex to effect repeat-specific processes. In the absence of PMS2, the inability of MSH2–MSH3 to signal downstream events would result in checkpoint-induced apoptotic removal of the germ cells, and subsequent infertility, but the absence of

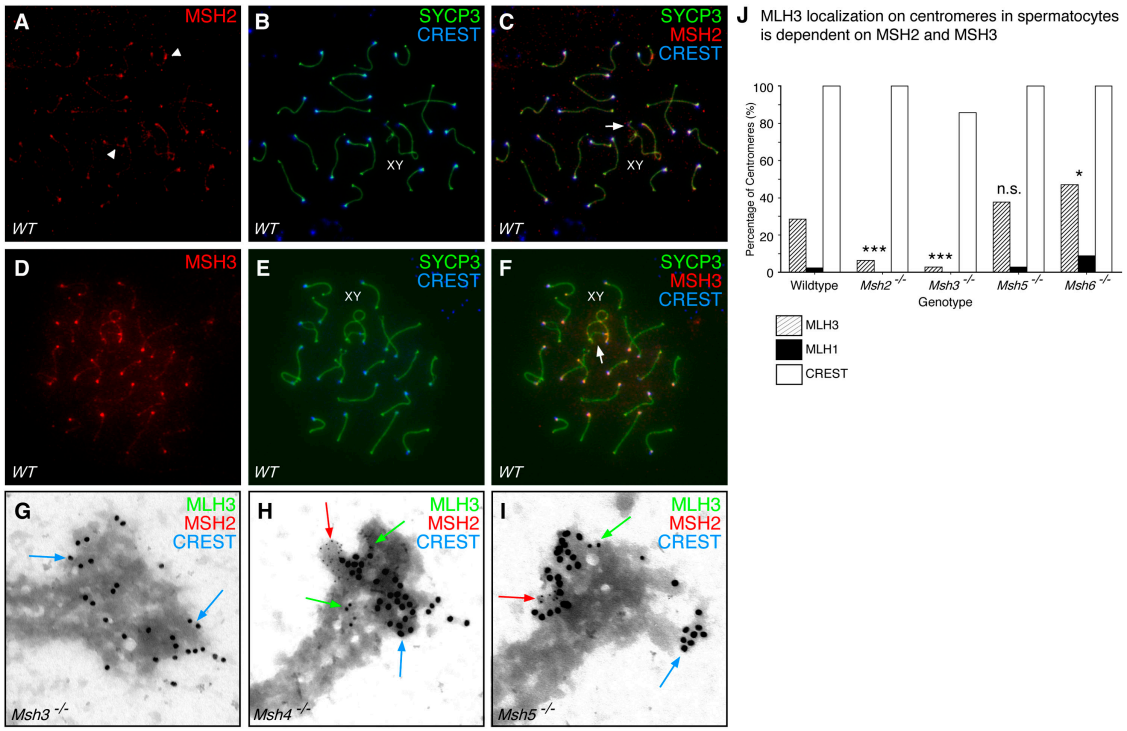

Figure 6. **Association of MMR proteins at centromere-associated and Y chromosome repeats is dependent on MutSβ (MSH2–MSH3).** (A-C) chromosome localization of MSH2 (red, TRITC) on wild-type SCs, as marked by SYCP3 (green, FITC) in association with the centromere, as marked by CREST labeling (blue, CY5), and the XY bivalent (C, arrow). MSH2 localization occurs at centromeres and the Y chromosome in spermatocytes from wild-type males (A–C; same cell in each panel), and is also found at occasional sites along the chromosome and throughout the chromatin area (see arrowheads in A). (D–F) MSH3 localization follows a similar pattern to MSH2, as shown in D (MSH3 is red, TRITC) and localizes most strongly with the CREST-positive regions (blue, CY5) in E and F, and also localizes to the XY (indicated by the arrow in F). (G–I) Immunogold electron micrographs showing the centromere regions of chromosomes from *Msh3*$^{-/-}$ (G), *Msh4*$^{-/-}$ (H), and *Msh5*$^{-/-}$ (I) spermatocytes in pachynema with MLH3 (12 nm gold beads, green), MSH2 (6 nm gold beads, red), and CREST (18 nm gold beads, blue) showing that the localization of MSH2 and MLH3 to this region is dependent on MSH3, but not on MSH4 and MSH5. (J) Quantitation of EM-gold localization of MLH3 (striped bars), MLH1 (filled bars), and CREST (empty bars) on spermatocyte centromeres from wild-type males, and males that are homozygous for mutations in *Msh2*, *Msh3*, *Msh5*, and *Msh6*. MLH3 localization is significantly decreased compared with wild type on centromeres from *Msh2*$^{-/-}$ and *Msh3*$^{-/-}$ spermatocytes, but not on centromeres from *Msh5*$^{-/-}$ or *Msh6*$^{-/-}$ spermatocytes. χ^2 analysis of MLH1 and MLH3 localization at spermatocyte centromeres reveals statistically significant differences between wild-type and both *Msh2*$^{-/-}$ and *Msh3*$^{-/-}$ males (***$P < 0.0002$), but not between wild-type and *Msh5*$^{-/-}$ males (not significant, n.s., $P = 0.81$). MLH3 levels were slightly increased at the centromeres of *Msh6*$^{-/-}$ spermatocytes (*$P = 0.043$).

MSH2 would prevent checkpoint activation and hence allow meiotic progression even in the absence of PMS2. If true, we hypothesized that the removal of MSH2 in the *Pms2*$^{-/-}$ males would restore spermatogenesis. To test this, we generated double-null males for *Msh2* and *Pms2*, and counted epididymal sperm in adult males. Sperm numbers in *Msh2*$^{-/-}$*Pms2*$^{+/-}$ males were close to that found in double heterozygous males (Table I). As expected, sperm numbers in *Msh2*$^{+/-}$*Pms2*$^{-/-}$ males was reduced to ~3.5% of normal, but swimming sperm were observed, albeit at a very reduced frequency (Table I). Sperm numbers in *Msh2*$^{-/-}$*Pms2*$^{-/-}$ were similar to that seen in *Pms2*$^{-/-}$ single nulls, with a few (8 out of a total of 1,102 sperm counted) swimming sperm. Thus, deletion of *Msh2* does not restore the fertility of *Pms2*$^{-/-}$ males.

Meiotic sexual dimorphism in Pms2$^{-/-}$ mice is related to alterations in MMR association with repetitive sequences at the centromere

During the course of these experiments, we sought to identify the basis for the sexually dimorphic meiotic phenotypes exhibited by male and female *Pms2*$^{-/-}$ mice. Interestingly, we observed no increase in MLH1–MLH3 association with centromeric repetitive sequences in prophase I oocytes from *Pms2*$^{-/-}$ females (Fig. 2 G). This suggests that, although hyperaccumulation of MLH proteins at male centromeres in the absence of PMS2 causes apoptosis, the absence of such accumulation in females does not trigger apoptosis. Thus, oocytes from *Pms2*$^{-/-}$ females are viable and the mice are fertile. Alternatively, in view of the hyperlocalization of the MMR proteins on the Y chromosome, we hypothesized that loss or destabilization of Y chromosome genes critical for spermatogenesis might result in spermatogenic failure specifically in males. However, microarray analysis of germ cell RNA through prophase I from *Pms2*$^{+/+}$ and *Pms2*$^{-/-}$ spermatocytes, using the 34,000 gene Affymetrix gene chips, revealed no specific changes in expression profiles of Y chromosome genes in the absence of PMS2, suggesting that the failure of spermatogenesis in *Pms2*$^{-/-}$ males is unlikely to be due to misexpression of spermatogenic genes residing on the Y chromosome. Instead, our data point to differential effects on MMR protein accumulation and/or functioning at centromere-associated repetitive sequences in male versus female *Pms2*-null mice.

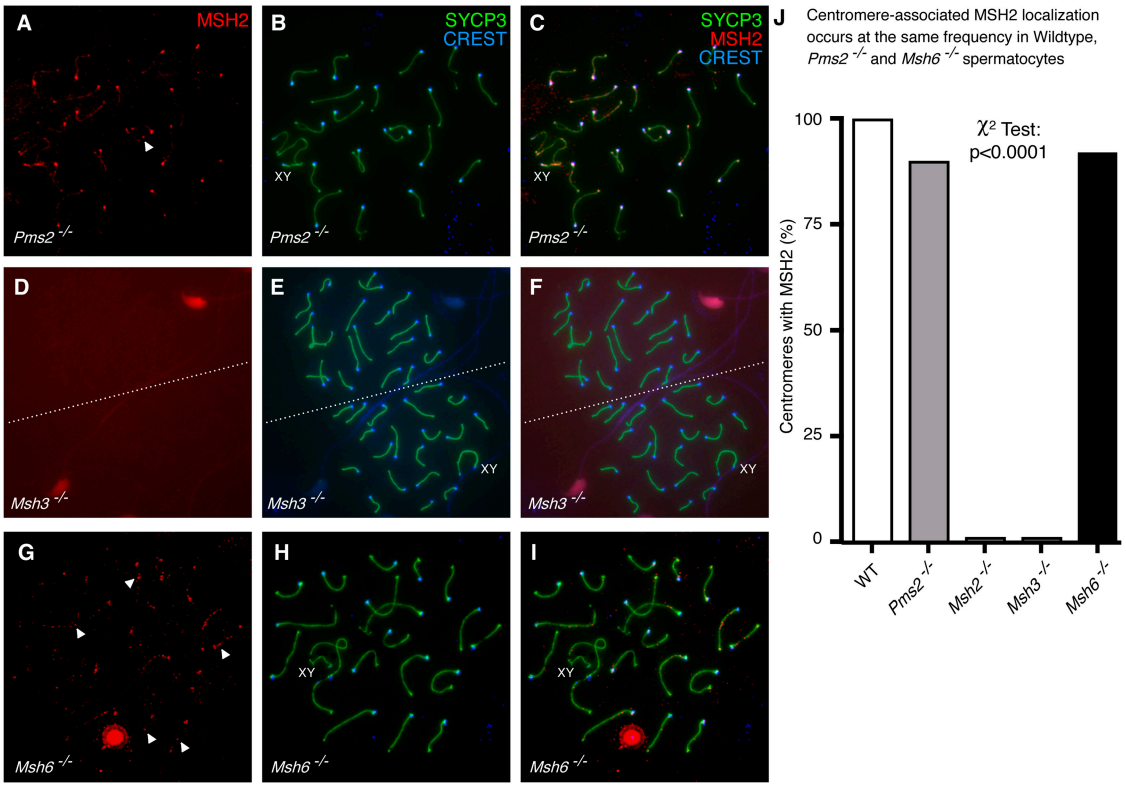

Figure 7. **Localization of MSH2 to the centromere regions of meiotic chromosomes is dependent on MSH3 but not MSH6 and PMS2.** (A–C) MSH2 localization to meiotic chromosome cores in a representative spermatocyte from a *Pms2*$^{-/-}$ male. MSH2 is localized in red (TRITC), SYCP3 in green (FITC) and the centromere in blue (CY5-CREST). Panel C shows the superimposed channels from panels A and B. (D–F) MSH2 localization to meiotic chromosomes in two representative spermatocytes from a *Msh3*$^{-/-}$ male. MSH2 is shown in red (TRITC), SYCP3 in green (FITC), and the centromere in blue (CY5-CREST). In the absence of MSH3, no MSH2 signal is apparent. (G–I) MSH2 localization to meiotic chromosomes in a representative spermatocyte from a *Msh6*$^{-/-}$ male. MSH2 is localized in red (TRITC), SYCP3 in green (FITC), and the centromere in blue (CY5-CREST). In A, D, and G, white arrowheads indicate interstitial localization of MSH2 along chromosome cores. (J) For each genotype, 5–10 cells were quantitated and the percentage of centromeres showing fluorescent signal for MSH2 was scored.

Discussion

The principal observations in this report include the following. First, the MLH1–MLH3 heterodimer appears to account for all the MNs found in late pachytene spermatocytes, a situation similar to that seen in yeast and their frequency is slightly elevated in the absence of PMS2. Second, MLH3 localizes to these sites before MLH1 and can associate with other regions of the genome independently of MLH1. Localization of MLH3 throughout the genome is substantially reduced but not eliminated in spermatocytes from *Mlh1*$^{-/-}$ males and is up-regulated in spermatocytes from *Pms2*$^{-/-}$ males. Third, MLH3 associates with repeat sequences around the centromere and on the Y chromosome during pachynema in spermatocytes from wild-type and *Mlh1*$^{-/-}$ males. This localization appears to differ from the localization at the MN sites because the pattern of distribution is not limited to chromosome cores, but instead appears diffuse and heterochromatic in its distribution. In addition, these sites do not appear to accumulate other DSB repair machinery components (such as RAD51; unpublished data), suggesting that DSBs are not forming at these sites. Fourth, the association of MLH3 with repeat sequences at the centromere is significantly increased, with almost all centromeres now being positive for MLH3. In addition, in the absence of PMS2, MLH1 associates with these MLH3 sites at repeat sequences. Fifth, the association of MLH3 (and MLH1) with repeat sequences at the centromere and on the Y chromosome during prophase I is dependent on MSH2 and MSH3, but not on MSH4, MSH5 or MSH6. Moreover, MSH2 localizes to these sites of repetitive sequence in all spermatocytes, both wild-type and *Pms2* null, and this localization is dependent on MSH3 (but not MSH4, 5, or 6).

Taken together these observations suggest that MLH1–MLH3 is the sole MutL heterodimer responsible for processing

Table I. **Epididymal sperm numbers in Msh2 and Pms2 single and double mutant animals**

Genotype	Sperm number	Percentage of normal	Number swimming
Msh2$^{+/-}$ Pms2$^{+/-}$	1.037×10^7 $\pm 0.931 \times 10^7$	100.0	ND
Msh2$^{-/-}$ Pms2$^{+/-}$	0.970×10^7 $\pm 0.331 \times 10^7$	93.5	ND
Msh2$^{+/-}$ Pms2$^{-/-}$	0.036×10^7 $\pm 0.030 \times 10^7$	3.5	1/525 (0.002%)
Msh2$^{-/-}$ Pms2$^{-/-}$	0.040×10^7 $\pm 0.015 \times 10^7$	3.9	8/1,102 (0.007%)

Values are means ± SD.
ND, not determined (assumed to be greater than 95%. Normal sperm samples had to be formalin fixed in order to be counted).

of meiotic crossovers and rule out a direct function for PMS2 in crossing over, paralleling the situation in *Saccharomyces cerevisiae* (Wang et al., 1999). In addition, these data demonstrate the existence of an additional meiotic MMR complex that associates specifically with sites of repetitive DNA at sites that are presumed to be refractory to reciprocal recombination events. It was not surprising, therefore, to find an MMR complex driven by MSH2–MSH3 instead of MSH4–MSH5. Also of significance is the fact that MLH3 can associate with chromosome regions independently of MLH1, suggesting the existence of a new MutL complex that is either stabilized by MLH1 or that can function independently of other MutL homologues. The MLH3-only complex could be inactive in terms of MMR activity, but could instead trigger alternative downstream events that would result in genome stabilization.

The up-regulation of centromere-associated MMR complexes in $Pms2^{-/-}$ males suggests that the absence of PMS2 facilitates the accumulation of repeat-associated MMR complexes, but does not necessarily point to any direct role for PMS2 at these sites. $Msh2^{-/-}$•$Pms2^{-/-}$ males are also sterile while $Msh2^{-/-}$ males are fertile, arguing against a role for PMS2 at the centromere. Instead, our results show that the loss of PMS2 results in an accumulation of the MSH2–MSH3–MLH1–MLH3 complex at sites of repetitive DNA as a secondary effect. We propose that PMS2 is working at other sites during spermatogenesis, in combination with MSH2, and that the loss of PMS2 at these sites leads to a redistribution of MMR complexes through the genome, resulting in increased association of MLH1–MLH3 with centromeric sequences (and, to a lesser extent, with sites of DSB processing). Alternatively, or in addition, the removal of PMS2 increases the need for MMR complexes at sites of repetitive DNA because of the general increase in genome instability in $Pms2^{-/-}$ mice. Moreover, we cannot rule out the possibility that the effect of *Pms2* deletion occurs at an earlier point in spermatogenesis, possibly during postreplicative repair at premeiotic S-phase, and that the meiotic failure is secondary to these earlier events. Indeed, Richardson et al. (2000) demonstrated high levels of mRNA and protein expression in mouse spermatogonia (Richardson et al., 2000), suggesting perhaps that PMS2 may be functioning at this earlier time in spermatogenesis.

Previous studies have suggested that tandem repeats, such as those found in human α satellite centromeric DNA, are susceptible to mispairing and other genome destabilizing events. They are conserved by gene conversion (Greig et al., 1993; Warburton et al., 1993; Schindelhauer and Schwarz, 2002), as are palindromic repeat units on the Y (Rozen et al., 2003; Skaletsky et al., 2003). Given that localization of MMR proteins to these sites is determined by MSH2–MSH3, our data support a function in noncrossover and/or repair events at these tandem repeat units, rather than a function in MSH4–MSH5-driven reciprocal recombination. In addition, the antirecombinational role of MSH2–MSH3 (Lin et al., 2004) could be beneficial at sites such as the centromere to prevent deleterious crossover events during prophase I, and may explain the high degree of conservation amongst centromere repeat regions.

The dynamics of MMR complex association with repetitive sequences at the centromere and on the Y chromosome during meiosis is reminiscent of the dynamics of MMR involvement in the expansion of simple trinucleotide repeat (TNR) sequences that give rise to complex disorders such as Huntington disease (Kovtun et al., 2001; Kovtun and McMurray, 2001) and myotonic dystrophy (van den Broek et al., 2002; Nag, 2003). The secondary structures that arise as a result of TNR misalignments are substrates for MSH2 (Pearson et al., 1997), and mutations in *Msh2* prevent CAG•CTG repeat expansion at the Huntington disease *Hdh* locus (Manley et al., 1999). In somatic cells, these events involve MSH3 because TNR expansion in myotonic dystrophy knock-in mice is abolished on a *Msh3*-null background (van den Broek et al., 2002). These MutSβ-dependent events, both in the germ line and in somatic cells, could involve canonical MMR and/or recombination processes or, as has been suggested, could instead result from the stabilization and protection from repair of CAG•CTG hairpin structures (Manley et al., 1999; Kovtun and McMurray, 2001) resulting from misalignment and looping of tandem triplet repeats (Moore et al., 1999).

Secondary looping structures could also play roles in MMR-driven events during meiosis. Heteroduplexes formed during recombination in yeast can include insertions as large as 5.6 kb in size (Kearney et al., 2001) and are targeted specifically by Msh2–Msh3 (Kearney et al., 2001). These substrates may induce very different biochemical events to the traditional MMR pathway and may therefore initiate a different cascade of downstream events. Moreover, long repeat tracts, involving triplet CAG motifs or large palindromes, induce DSB formation during yeast meiosis (Jankowski et al., 2000; Nasar et al., 2000; Nag, 2003) that could give rise to recombinational repair events. This raises the possibility that the repeat tracts and palindromes in the centromere regions and on the Y chromosome could present similar recombinational substrates during murine meiosis, inducing DSBs in late pachynema through the action of SPO11, which is still present during that time (Keeney et al., 1999; Romanienko and Camerini-Otero, 1999), that then need to be repaired by recombinational events, with a preference for noncrossover mechanisms. However, this possibility is tempered by the failure to detect other DSB repair machinery components (RAD51) at these sites (unpublished data).

In conclusion, our results suggest a novel function for the MMR machinery during mammalian meiosis, whereby MSH2–MSH3 are present as a surveillance mechanism, to restore repeat frequency, through stabilization/maintenance of hairpin structures present within the context of tandem repeats, and/or through suppression of reciprocal recombination events resulting from secondary structure–induced DSB formation, that could result in chromosomal translocations, enlarged loops, and other cytogenetic errors. Should repeat units become misaligned or out of register, a resulting single stranded loop structure would be detected by the surveillance complex and would activate downstream (repair) events involving, at the very least, MLH3, and that would ultimately effect the restoration of unit numbers.

Materials and methods

Animals

The generation of mouse mutants for *Pms2, Mlh1, Mlh3, Msh2, Msh3, Msh4, Msh5,* and *Msh6* have been described previously, along with

genotyping strategies for each strain (Baker et al., 1995; Edelmann et al., 1996, 1999, 2000; Kneitz et al., 2000; Lipkin et al., 2002). All strains were housed in the Albert Einstein College of Medicine Animal Institute on standardized light, heat, and feeding schedules. All strains were maintained on similar backgrounds by backcrossing heterozygote fathers with C57Bl/6J mothers.

Chromosome preparations

The standard chromosome spreading protocol has been described previously for our laboratory (Lenzi et al., 2005). The nuclear contents of whole-mount spermatocytes (or oocytes) were displayed by drying down a cell suspension, in hypotonic buffer, from either testis, or ovary, in 1% paraformaldehyde containing 0.15% Triton X-100 (Peters et al., 1997). Whole testes or ovaries were incubated on ice for 60 min in hypotonic extraction buffer (HEB; 30 mM Tris, pH 8.2, 50 mM sucrose, 17 mM trisodium citrate dihydrate, 5 mM EDTA, 0.5 mM DTT, and 0.5 mM PMSF). Either a one-inch length of tubule, or a whole ovary, were placed in a 20-μl drop of 100 mM sucrose, pH 8.2, the tissue was macerated, and a second 20-μl drop of sucrose solution was added and the cell suspension was pipetted up and down several times. Remnant pieces of tubule were removed. Cleaned slides were dipped in the paraformaldehyde and Triton X-100 solution, and most liquid was drained off, such that only enough liquid remained to coat the slide. 20 μl of the cell suspension was added in one corner and the cells were slowly dispersed, first in a horizontal direction and then vertical. The remaining 20 μl of cell suspension was used to make a second slide and both were placed in a humid chamber to dry slowly at RT for 2 h. The slides were washed three times for 1 min in 0.4% Kodak Photo-Flo 200 and air dried for at least 15 min. For EM preparations, to make the SCs accessible to immunogold grains, the slides were DNaseI treated (1 μl/ml of DMEM) before being air dried (Moens et al., 2002). The slides were washed and blocked (three times for 10 min each) in PBS and incubated in primary antibodies overnight at RT in a humid chamber. Primary antibodies were used at varying concentrations, and generally a 10-fold higher concentration was used for EM than immunofluorescence. After washes, slides were incubated in secondary antibodies, conjugated to either fluorochrome or colloidal gold (Jackson ImmunoResearch Laboratories), for 2 h at 37°C. After washes the slides were mounted with ProLong Antifade (Invitrogen) for fluorescence microscopy. Images were captured on a Olympus IX81 microscope attached to a 12-bit Cooke Sensicam CCD instrument and sent to IP Lab software.

For EM, slides were incubated in 4% alcoholic phosphotungstic acid for 15 min, followed by three 1-min washes in 95% ethanol, to enhance visualization of MNs. Slides were air dried and then dipped in 0.25% formvar (Electron Microscopy Sciences) and air dried under glass. The plastic was scored, treated with 25% hydrofluoric acid, and floated off in water with attached cells. Plastic was transferred to EM grids and used for transmission EM (JEOL 1200EX).

Antibodies

The numerous antibodies used were obtained from a variety of sources: mouse anti–human MLH1 antibody (BD Biosciences, clone G168-15); mouse anti–human MSH2 (clone G219-1129; BD Biosciences); and mouse anti–human MSH3 (clone 52; BD Biosciences). In addition, the following antibodies have been generated in our laboratory or by our collaborators: rabbit anti-MLH3 (Lipkin et al., 2002), rabbit anti–hamster COR1 to detect SYCP3 (Lenzi et al., 2005), and mouse anti–hamster COR1 (Lenzi et al., 2005).

Quantitation and statistical analysis

Immunofluorescence chromosome counts and cell staging were performed by at least three independent observers, compiled using Excel, and then analyzed using the statistical software package, Prism 3.0 (GraphPad Software). Staging of prophase I cells was performed using well-defined criteria for SC morphology, XY synapsis, and double dense body (DDB) and sex body status (Ashley and Plug, 1998; Moens et al., 2002). For such studies, we used previously published criteria (Dresser et al., 1987; Allen et al., 1988; Backer et al., 1988). Pachynema was divided into early, mid, and late stages on the basis of chromosome appearance, degree of compaction, XY status, and DDB formation. In early pachynema, the XY is synapsed along most of the length of the PAR and much of the X chromosome appears synapsed. Small regions of the autosomes may not be synapsed at this point. By mid-pachynema, the autosomes are completely synapsed and further compacted, whereas the XY is synapsed up to ~20% of the length of the X chromosomes. The DDB appears at this time and the sex body becomes apparent. By late pachynema, only the tip of the PAR remains synapsed, the sex body is much more distinct, and the DDB is still present. Note that the MLH3 (and MLH1) signal found at the centromere was not included in our MN focus counts depicted in Fig. 1 and that these populations are, we believe, distinct from one another.

Gold grain counts of centromere-associated proteins were counted at the EM level. For each staining preparation, counts were made from spermatocytes of at least three animals, with no fewer than 200 centromeres counted per animal, including up to 19 autosomes from a single cell being counted. In some cases fewer autosomes were counted in cells whose total chromosome count was not completely visible. Equivalent telomere counts were performed for each preparation as matched controls. In all cases, the number of centromeres/telomeres having one, two or three, or more than four gold grains were tabulated, but the threshold for specificity was set at more than four gold grains.

Chromatin immunoprecipitation

Adult testes were decapsulated, placed in a drop of cell culture media, minced, and seminiferous tubules squeezed to release germ cells. Alternatively, pure populations of pachytene spermatocytes were obtained by sedimentation velocity gradient ("STA-PUT"; Romrell et al., 1976). Germ cells were taken up in 1 ml of cell culture media and cross-linking was performed at RT for 5 min by addition of formaldehyde to 1% concentration. Cross-linking was stopped by addition of glycine to 0.125 M. Cells were collected by centrifugation, washed in PBS, and lysed in 1 ml of FA lysis buffer (50 mM Hepes, 150 mM NaCl, 1 mM EDTA, 1% Triton X-100, 0.1% sodium deoxycholate, 0.1% SDS, pH 7.5) with addition of protease inhibitors. Cell lysates were sonicated eight times for 20 s each at 20% output setting, and lysates were cleared of cell debris by centrifugation. For each immunoprecipitation 1/10 of the total testis lysate volume was diluted 10 times in FA buffer and precleared with 2 μg sheared salmon sperm DNA, 10 μl of preimmune serum and protein A/G-Sepharose slurry for 1 h at 4°C. Immunoprecipitation was performed overnight at 4°C with specific antibodies. After immunoprecipitation, protein A/G-Sepharose slurry was added and the incubation was continued for 1 h. Precipitates were washed sequentially for 5 min each in FA buffer, FA buffer with 0.5 M NaCl, LiCl wash buffer (10 mM TrisCl, 0.25 M LiCl, 1 mM EDTA, 0.5% Nonidet P-40, 0.5% sodium deoxycholate), and TE buffer. The immune complexes were eluted from the beads by addition of 50 mM Tris, 10 mM EDTA, 1% SDS. Cross-linking was reversed by incubation at 65°C for at least 6 h DNA fragments were purified by phenol-chloroform-isoamyl alcohol extraction and ethanol precipitation. Equal aliquots from each immunoprecipitation were amplified using degenerate oligonucleotide PCR method of Telenius et al. (1992). Products of amplification were analyzed by slot-blot hybridization, using "North2South" hybridization kit (Pierce Chemical Co.). Probes for hybridization were generated by PCR according to published sequences for the mouse minor and major satellite probe (Garagna et al., 2002), B2 SINE element probe (Serdobova and Kramerov, 1998), and mouse Y chromosome–specific LINE-1 probe (DYzEms10 locus; Navin et al., 1996).

Online supplemental material

Two figures are presented as supplemental data items. Fig. S1 shows MLH3 localization at the centromere of spermatocytes from *Pms2*$^{-/-}$ males. Fig. S2 provides validation of ChIP experiments used in this study. Online supplemental materials are available at http://www.jcb.org/cgi/content/full/jcb.200506170/DC1.

The authors acknowledge, with gratitude, Dr. Stefan Scherer for guidance in looking at somatic cell centromere behavior.

This work was funded by the National Institute of Child Health and Development (RO1HD41012-01), The March of Dimes Birth Defects Foundation (MOD-FY2002-282), and by start-up funding from the Albert Einstein College of Medicine to P.E. Cohen and by the National Cancer Institute (R01CA76329) to W. Edelmann. At the time that this work was conducted, A. Svetlanov was supported by training grant sponsorship to the Albert Einstein College of Medicine from The National Institute of General Medical Sciences (T32 GM 07491).

Submitted: 27 June 2005
Accepted: 4 October 2005

References

Allen, J.W., P.A. Poorman, L.C. Backer, J.B. Gibson, B. Westbrook-Collins, and M.J. Moses. 1988. Synaptonemal complex damage as a measure of

genotoxicity at meiosis. *Cell Biol. Toxicol.* 4:487–494.

Anderson, L.K., A. Reeves, L.M. Webb, and T. Ashley. 1999. Distribution of crossing over on mouse synaptonemal complexes using immunofluorescent localization of MLH1 protein. *Genetics.* 151:1569–1579.

Ashley, T., and A. Plug. 1998. Caught in the act: deducing meiotic function from protein immunolocalization. *Curr. Top. Dev. Biol.* 37:201–239.

Backer, L.C., J.B. Gibson, M.J. Moses, and J.W. Allen. 1988. Synaptonemal complex damage in relation to meiotic chromosome aberrations after exposure of male mice to cyclophosphamide. *Mutat. Res.* 203:317–330.

Baker, S.M., C.E. Bronner, L. Zhang, A.K. Plug, M. Robatzek, G. Warren, E.A. Elliott, J. Yu, T. Ashley, N. Arnheim, et al. 1995. Male mice defective in the DNA mismatch repair gene *PMS2* exhibit abnormal chromosome synapsis in meiosis. *Cell.* 82:309–319.

Baker, S.M., A.W. Plug, T.A. Prolla, C.E. Bronner, A.C. Harris, X. Yao, D.M. Christie, C. Monell, N. Arnheim, A. Bradley, et al. 1996. Involvement of mouse Mlh1 in DNA mismatch repair and meiotic crossing over. *Nat. Genet.* 13:336–342.

Bishop, C.E., P. Boursot, B. Baron, F. Bonhomme, and D. Hatat. 1985. Most classical Mus musculus domesticus laboratory mouse strains carry a Mus musculus musculus Y chromosome. *Nature.* 315:70–72.

Borner, G.V., N. Kleckner, and N. Hunter. 2004. Crossover/noncrossover differentiation, synaptonemal complex formation, and regulatory surveillance at the leptotene/zygotene transition of meiosis. *Cell.* 117:29–45.

Broman, K.W., J.C. Murray, V.C. Sheffield, R.L. White, and J.L. Weber. 1998. Comprehensive human genetic maps: individual and sex-specific variation in recombination. *Am. J. Hum. Genet.* 63:861–869.

de Vries, S.S., E.B. Baart, M. Dekker, A. Siezen, D.G. de Rooij, P. de Boer, and H. te Riele. 1999. Mouse MutS-like protein Msh5 is required for proper chromosome synapsis in male and female meiosis. *Genes Dev.* 13:523–531.

Dresser, M., D. Pisetsky, R. Warren, G. McCarty, and M. Moses. 1987. A new method for the cytological analysis of autoantibody specificities using whole-mount, surface-spread meiotic nuclei. *J. Immunol. Methods.* 104:111–121.

Edelmann, W., P.E. Cohen, M. Kane, K. Lau, B. Morrow, S. Bennett, A. Umar, T. Kunkel, G. Cattoretti, R. Chaganti, et al. 1996. Meiotic pachytene arrest in MLH1-deficient mice. *Cell.* 85:1125–1134.

Edelmann, W., P.E. Cohen, B. Kneitz, N. Winand, M. Lia, J. Heyer, R. Kolodner, J.W. Pollard, and R. Kucherlapati. 1999. Mammalian MutS homologue 5 is required for chromosome pairing in meiosis. *Nat. Genet.* 21:123–127.

Edelmann, W., A. Umar, K. Yang, J. Heyer, M. Kucherlapati, M. Lia, B. Kneitz, E. Avdievich, K. Fan, E. Wong, et al. 2000. The DNA mismatch repair genes Msh3 and Msh6 cooperate in intestinal tumor suppression. *Cancer Res.* 60:803–807.

Flores-Rozas, H., and R.D. Kolodner. 1998. The *Saccharomyces cerevisiae* MLH3 gene functions in MSH3-dependent suppression of frameshift mutations. *Proc. Natl. Acad. Sci. USA.* 95:12404–12409.

Flores-Rozas, H., and R.D. Kolodner. 2000. Links between replication, recombination and genome instability in eukaryotes. *Trends Biochem. Sci.* 25:196–200.

Froenicke, L., L.K. Anderson, J. Wienberg, and T. Ashley. 2002. Male mouse recombination maps for each autosome identified by chromosome painting. *Am. J. Hum. Genet.* 71:1353–1368.

Garagna, S., M. Zuccotti, E. Capanna, and C.A. Redi. 2002. High-resolution organization of mouse telomeric and pericentromeric DNA. *Cytogenet. Genome Res.* 96:125–129.

Greig, G.M., P.E. Warburton, and H.F. Willard. 1993. Organization and evolution of an alpha satellite DNA subset shared by human chromosomes 13 and 21. *J. Mol. Evol.* 37:464–475.

Guenatri, M., D. Bailly, C. Maison, and G. Almouzni. 2004. Mouse centric and pericentric satellite repeats form distinct functional heterochromatin. *J. Cell Biol.* 166:493–505.

Hoffmann, E.R., and R.H. Borts. 2004. Meiotic recombination intermediates and mismatch repair proteins. *Cytogenet. Genome Res.* 107:232–248.

Hollingsworth, N.M., L. Ponte, and C. Halsey. 1995. MSH5, a novel MutS homolog, facilitates meiotic reciprocal recombination between homologs in *Saccharomyces cerevisiae* but not mismatch repair. *Genes Dev.* 9:1728–1739.

Horz, W., and W. Altenburger. 1981. Nucleotide sequence of mouse satellite DNA. *Nucleic Acids Res.* 9:683–696.

Jankowski, C., F. Nasar, and D.K. Nag. 2000. Meiotic instability of CAG repeat tracts occurs by double-strand break repair in yeast. *Proc. Natl. Acad. Sci. USA.* 97:2134–2139.

Kearney, H.M., D.T. Kirkpatrick, J.L. Gerton, and T.D. Petes. 2001. Meiotic recombination involving heterozygous large insertions in *Saccharomyces cerevisiae*: formation and repair of large, unpaired DNA loops. *Genetics.* 158:1457–1476.

Keeney, S., F. Baudat, M. Angeles, Z.H. Zhou, N.G. Copeland, N.A. Jenkins, K. Manova, and M. Jasin. 1999. A mouse homolog of the *Saccharomyces cerevisiae* meiotic recombination DNA transesterase Spo11p. *Genomics.* 61:170–182.

Kirkpatrick, D.T. 1999. Roles of the DNA mismatch repair and nucleotide excision repair proteins during meiosis. *Cell. Mol. Life Sci.* 55:437–449.

Kneitz, B., P.E. Cohen, E. Avdievich, L. Zhu, M.F. Kane, H. Hou Jr., R.D. Kolodner, R. Kucherlapati, J.W. Pollard, and W. Edelmann. 2000. MutS homolog 4 localization to meiotic chromosomes is required for chromosome pairing during meiosis in male and female mice. *Genes Dev.* 14:1085–1097.

Kolodner, R. 1996. Biochemistry and genetics of eukaryotic mismatch repair. *Genes Dev.* 10:1433–1442.

Kolodner, R.D., and G.T. Marsischky. 1999. Eukaryotic DNA mismatch repair. *Curr. Opin. Genet. Dev.* 9:89–96.

Kovtun, I.V., and C.T. McMurray. 2001. Trinucleotide expansion in haploid germ cells by gap repair. *Nat. Genet.* 27:407–411.

Kovtun, I.V., G. Goellner, and C.T. McMurray. 2001. Structural features of trinucleotide repeats associated with DNA expansion. *Biochem. Cell Biol.* 79:325–336.

Lenzi, M.L., J. Smith, T. Snowden, M. Kim, R. Fishel, B.K. Poulos, and P.E. Cohen. 2005. Extreme heterogeneity in the molecular events leading to the establishment of chiasmata during meiosis i in human oocytes. *Am. J. Hum. Genet.* 76:112–127.

Lin, D.P., Y. Wang, S.J. Scherer, A.B. Clark, K. Yang, E. Avdievich, B. Jin, U. Werling, T. Parris, N. Kurihara, et al. 2004. An Msh2 point mutation uncouples DNA mismatch repair and apoptosis. *Cancer Res.* 64:517–522.

Lipkin, S.M., P.B. Moens, V. Wang, M. Lenzi, D. Shanmugarajah, A. Gilgeous, J. Thomas, J. Cheng, J.W. Touchman, E.D. Green, et al. 2002. Meiotic arrest and aneuploidy in MLH3-deficient mice. *Nat. Genet.* 31:385–390.

Manley, K., T.L. Shirley, L. Flaherty, and A. Messer. 1999. Msh2 deficiency prevents in vivo somatic instability of the CAG repeat in Huntington disease transgenic mice. *Nat. Genet.* 23:471–473.

Modrich, P. 1997. Strand-specific mismatch repair in mammalian cells. *J. Biol. Chem.* 272:24727–24730.

Moens, P.B., N.K. Kolas, M. Tarsounas, E. Marcon, P.E. Cohen, and B. Spyropoulos. 2002. The time course and chromosomal localization of recombination-related proteins at meiosis in the mouse are compatible with models that can resolve the early DNA-DNA interactions without reciprocal recombination. *J. Cell Sci.* 115:1611–1622.

Moore, H., P.W. Greenwell, C.P. Liu, N. Arnheim, and T.D. Petes. 1999. Triplet repeats form secondary structures that escape DNA repair in yeast. *Proc. Natl. Acad. Sci. USA.* 96:1504–1509.

Muro, Y., H. Masumoto, K. Yoda, N. Nozaki, M. Ohashi, and T. Okazaki. 1992. Centromere protein B assembles human centromeric alpha-satellite DNA at the 17-bp sequence, CENP-B box. *J. Cell Biol.* 116:585–596.

Nag, D.K. 2003. Trinucleotide repeat expansions: timing is everything. *Trends Mol. Med.* 9:455–457.

Nakagawa, T., A. Datta, and R.D. Kolodner. 1999. Multiple functions of MutS- and MutL-related heterocomplexes. *Proc. Natl. Acad. Sci. USA.* 96:14186–14188.

Nasar, F., C. Jankowski, and D.K. Nag. 2000. Long palindromic sequences induce double-strand breaks during meiosis in yeast. *Mol. Cell. Biol.* 20:3449–3458.

Navin, A., R. Prekeris, N.A. Lisitsyn, M.M. Sonti, D.A. Grieco, S. Narayanswami, E.S. Lander, and E.M. Simpson. 1996. Mouse Y-specific repeats isolated by whole chromosome representational difference analysis. *Genomics.* 36:349–353.

Novak, J.E., P.B. Ross-Macdonald, and G.S. Roeder. 2001. The budding yeast Msh4 protein functions in chromosome synapsis and the regulation of crossover distribution. *Genetics.* 158:1013–1025.

Page, S.L., and R.S. Hawley. 2004. The genetics and molecular biology of the synaptonemal complex. *Annu. Rev. Cell Dev. Biol.* 20:525–558.

Pearson, C.E., A. Ewel, S. Acharya, R.A. Fishel, and R.R. Sinden. 1997. Human MSH2 binds to trinucleotide repeat DNA structures associated with neurodegenerative diseases. *Hum. Mol. Genet.* 6:1117–1123.

Peters, A.H., A.W. Plug, M.J. van Vugt, and P. de Boer. 1997. A drying-down technique for the spreading of mammalian meiocytes from the male and female germline. *Chromosome Res.* 5:66–68.

Qin, J., S. Baker, H. Te Riele, R.M. Liskay, and N. Arnheim. 2002. Evidence for the lack of mismatch-repair directed antirecombination during mouse meiosis. *J. Hered.* 93:201–205.

Richardson, L.L., C. Pedigo, and M.A. Handel. 2000. Expression of deoxyribonucleic acid repair enzymes during spermatogenesis in mice. *Biol. Reprod.* 62:789–796.

Romanienko, P.J., and R.D. Camerini-Otero. 1999. Cloning, characterization,

and localization of mouse and human SPO11. *Genomics.* 61:156–169.

Romrell, L.J., A.R. Bellve, and D.W. Fawcett. 1976. Separation of mouse spermatogenic cells by sedimentation velocity. A morphological characterization. *Dev. Biol.* 49:119–131.

Ross-Macdonald, P., and G.S. Roeder. 1994. Mutation of a meiosis-specific MutS homolog decreases crossing over but not mismatch correction. *Cell.* 79:1069–1080.

Rozen, S., H. Skaletsky, J.D. Marszalek, P.J. Minx, H.S. Cordum, R.H. Waterston, R.K. Wilson, and D.C. Page. 2003. Abundant gene conversion between arms of palindromes in human and ape Y chromosomes. *Nature.* 423:873–876.

Santucci-Darmanin, S., D. Walpita, F. Lespinasse, C. Desnuelle, T. Ashley, and V. Paquis-Flucklinger. 2000. MSH4 acts in conjunction with MLH1 during mammalian meiosis. *FASEB J.* 14:1539–1547.

Schindelhauer, D., and T. Schwarz. 2002. Evidence for a fast, intrachromosomal conversion mechanism from mapping of nucleotide variants within a homogeneous alpha-satellite DNA array. *Genome Res.* 12:1815–1826.

Serdobova, I.M., and D.A. Kramerov. 1998. Short retroposons of the B2 superfamily: evolution and application for the study of rodent phylogeny. *J. Mol. Evol.* 46:202–214.

Silver, L.M. 1995. Mouse Genetics: Concepts and Applications. Oxford University Press, New York. 362 pp.

Singh, L., S.G. Panicker, R. Nagaraj, and K.C. Majumdar. 1994. Banded krait minor-satellite (Bkm)-associated Y chromosome-specific repetitive DNA in mouse. *Nucleic Acids Res.* 22:2289–2295.

Skaletsky, H., T. Kuroda-Kawaguchi, P.J. Minx, H.S. Cordum, L. Hillier, L.G. Brown, S. Repping, T. Pyntikova, J. Ali, T. Bieri, et al. 2003. The male-specific region of the human Y chromosome is a mosaic of discrete sequence classes. *Nature.* 423:825–837.

Snowden, T., S. Acharya, C. Butz, M. Berardini, and R. Fishel. 2004. hMSH4-hMSH5 recognizes Holliday junctions and forms a meiosis-specific sliding clamp that embraces homologous chromosomes. *Mol. Cell.* 15:437–451.

Surtees, J.A., J.L. Argueso, and E. Alani. 2004. Mismatch repair proteins: key regulators of genetic recombination. *Cytogenet. Genome Res.* 107:146–159.

Telenius, H., N.P. Carter, C.E. Bebb, M. Nordenskjold, B.A. Ponder, and A. Tunnacliffe. 1992. Degenerate oligonucleotide-primed PCR: general amplification of target DNA by a single degenerate primer. *Genomics.* 13:718–725.

van den Broek, W.J., M.R. Nelen, D.G. Wansink, M.M. Coerwinkel, H. te Riele, P.J. Groenen, and B. Wieringa. 2002. Somatic expansion behaviour of the (CTG)n repeat in myotonic dystrophy knock-in mice is differentially affected by Msh3 and Msh6 mismatch-repair proteins. *Hum. Mol. Genet.* 11:191–198.

Wang, T.F., N. Kleckner, and N. Hunter. 1999. Functional specificity of MutL homologs in yeast: evidence for three Mlh1-based heterocomplexes with distinct roles during meiosis in recombination and mismatch correction. *Proc. Natl. Acad. Sci. USA.* 96:13914–13919 (see comments).

Warburton, P.E., J.S. Waye, and H.F. Willard. 1993. Nonrandom localization of recombination events in human alpha satellite repeat unit variants: implications for higher-order structural characteristics within centromeric heterochromatin. *Mol. Cell. Biol.* 13:6520–6529.

Winand, N.J., J.A. Panzer, and R.D. Kolodner. 1998. Cloning and characterization of the human and *Caenorhabditis elegans* homologs of the *Saccharomyces cerevisiae* MSH5 gene. *Genomics.* 53:69–80.

Woods, L.M., C.A. Hodges, E. Baart, S.M. Baker, R.M. Liskay, and P.A. Hunt. 1999. Chromosomal influence on meiotic spindle assembly: abnormal meiosis I in female Mlh1 mutant mice. *J. Cell Biol.* 145:1395–1406.

Zalevsky, J., A.J. MacQueen, J.B. Duffy, K.J. Kemphues, and A.M. Villeneuve. 1999. Crossing over during *Caenorhabditis elegans* meiosis requires a conserved MutS-based pathway that is partially dispensable in budding yeast. *Genetics.* 153:1271–1283.